

A Computational Aerodynamic Study of Tandem Rotating Wheels in Contact with the Ground

Mohammad Rasidi Rasani*, Azhari Shamsudeen, Zambri Harun and Wan Mohd Faizal Wan Mahmood

Center of Integrated Design for Advanced Mechanical Systems
Faculty of Engineering and Built Environment
Universiti Kebangsaan Malaysia, 43600 Bangi, Malaysia
*Corresponding author Email: rasidi@ukm.edu.my

Abstract

Wheels have significant impact on noise and drag of road vehicles, which may influence their fuel consumption, emission and comfort. A number of studies have analyzed flow and aerodynamics of isolated wheel in contact with the ground, but limited attention has been given to interaction between wheels. The present study aims to compare the aerodynamics and flow structure between single and tandem wheels. To that end, flow around single and tandem wheels are simulated using a turbulence Scaled Adaptive Unsteady Reynolds Average Navier Stokes (URANS) model. Wheel geometry was based on the actual wheel used in the experiments of Fackrell and Harvey. Flow around single and tandem wheels were examined and compared, along with their respective drag and lift coefficients. Results for single wheel in contact with the ground show good agreement with previous experiments. In the tandem wheel case, the rear wheel exhibits lower drag coefficient ($CD = 0.37$) and more downforce (lift coefficient $CL = -0.14$) compared to the front wheel. The present investigation may help to illustrate impact of wheel interaction on their aerodynamics.

Keywords: Tandem wheels; Rotating wheel; Aerodynamic; Computational fluid dynamics (CFD); Scale adaptive turbulence simulation.

1. Introduction

Fuel consumption and emission are two of many major concerns in the automotive industry. Minimizing vehicle drag may help to reduce fuel consumption and hence, emission from a road vehicle. Flow around wheels can have significant influence on flow features around a vehicle and on their drag. In particular, wheels contribute about 40% to total drag of open-wheeled racing cars [1] and wheels may contribute up to 25% of total drag in passenger cars [2,3]. Wheels also contribute significantly to noise in road cars and trucks [4,5]. Hence, understanding flow around wheels is clearly important in design of road vehicles, especially for minimizing vehicle drag that may contribute to lower fuel consumption and emission, and for minimizing noise that may improve driving comfort.

As a result, a number of studies concerning flow around wheels have been undertaken, especially for isolated wheel. McManus and Zhang performed Unsteady Reynolds Averaged Navier Stokes (URANS) simulation on a stationary and rotating isolated wheel in contact with the ground [5]. Their computations showed good agreement with experimental results of Fackrell and Harvey [6] and established difference in mean flow structures between a stationary and rotating wheel. Unlike McManus and Zhang [5] who examined slick tyres, Leśniewicz et al. [7] simulated both slick and grooved isolated rotating wheel using URANS computations, and showed reduced drag on grooved tyre, with presence of negative pressure at wheel-ground contact region as flow is accelerated through those grooves. Apart from widely used URANS models, Large Eddy Simulation (LES) and Detached Eddy Simulation (DES) have also been performed on isolated rotating wheel, reveal-

ing more detailed flow structures around hub and wake regions [8]. Their results showed interaction between flow structures in the hub with those around the lower separation region as the wheel rotates, leading to wider spread of lower separation vortices. In contrast, Axerio et al. [9] simulated both steady RANS and LES computations of an isolated stationary wheel and compared them to their PIV results. From the literature, although LES computations may be more accurate especially at regions of highly separated flows, URANS models were adequate to capture tyre surface pressure distribution and important mean flow structures around the tyre (for instance, arch-shaped trailing vortices in the upper wake region and counter-rotating vortex pairs in the far wake region).

In contrast to computational studies, direct measurement of wheel lift and drag forces in wind tunnel experiments have been affected by varying contact forces between the wheel and the moving ground. However, indirect method of deriving aerodynamic forces by measuring wheel surface pressure were more successful, as presented by the widely referenced benchmark experiments of Fackrell [10] and Fackrell & Harvey [6] for an isolated rotating wheel in contact with a moving ground. Their experiments confirmed results from earlier attempts at directly measuring aerodynamic forces on a wheel and suggested a peak surface pressure just upstream of the wheel-ground contact as a result of flow being forced towards this contact region before 'jetting' out through sides of the rotating wheel.

Wheels arranged in tandem may be found in many trucks and buses. Although many investigations have examined the aerodynamics of isolated wheels, flow around tandem wheels have received less attention. Indeed, a wind tunnel experiment on tandem

wheels were performed just recently by Spagnolo et al. in 2017 [11]. Therefore, in the present article, we aim to study the aerodynamics around tandem wheels and examine their flow in comparison to an isolated wheel. To that end, we simulate flow around a rotating single and tandem wheels in contact with the ground using a newly developed scale resolving or scale adaptive URANS turbulence model, proposed by Menter & Egorov [12].

2. Methodology

Numerical experiments involving single and tandem wheels were undertaken in the present study. In the following, further details of the computational model and simulation are briefly presented.

2.1. Wheel Geometry

To facilitate the comparison with experimental data, the wheel geometry chosen was based on an actual slick tyre described as 'A2' configuration in the experiments by Fackrell and Harvey [6,10]. The wheel has a diameter of $D = 416$ mm and a shoulder breadth of 185.4 mm. A contact patch between the wheel and the ground is also defined. In the present study, the gap between the tandem wheels is kept at $0.5D$.

2.2 Computational Grid

Figure 1 shows the geometry of the computational domain that was defined to closely follow previous successful studies. The forward wheel is located $5D$ downstream of the inlet and is $15D$ away from the outlet boundary. Height and width of the computational grid is set to $3.5D$ and $4D$ respectively. The computational grid is divided into 2 blocks or sub-domains: an inner block enclosing the wheels and the outer block away from the wheels. Finer grid resolution were employed in the inner block surrounding the wheels in order to capture the necessary flow features and rapid changes in flow variables in the vicinity and wake regions of the wheels. Grids were also clustered close to the wheel surface and moving ground to resolve their boundary layers, with maximum y^+ around the wheel approximately 2.6 except near the contact patch where a maximum y^+ of 3.5 may be obtained. It is remarked that a very thin 2 mm platform is extended from the wheel-ground contact patch, in order to preserve boundary layer mesh quality. This is important to accurately capture boundary layer flow near the wheel-ground contact region. In total, 2.39 million cells and 3.89 million cells were employed in the single and tandem wheel simulations respectively. Figure 2 shows the computational grid in the present study.

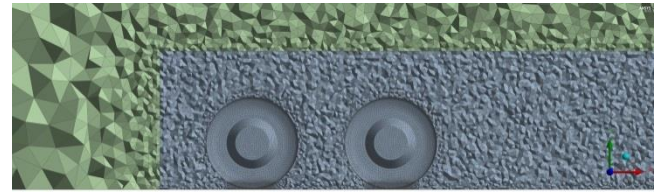


Fig. 1: Computational domain in the present study for tandem wheel case (for single wheel case, rear wheel is not included).

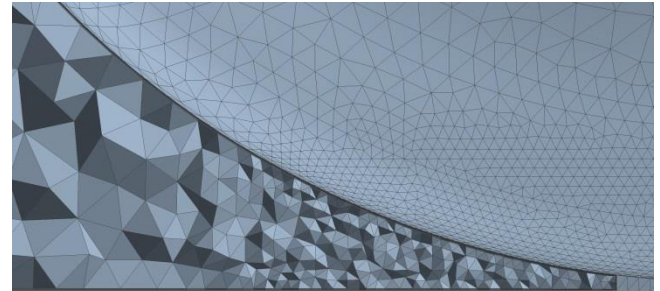
2.3 Flow and Boundary Conditions

The computations were undertaken at similar flow conditions to those in the experiments by Fackrell and Harvey [6,10] which was at Reynolds number based on wheel diameter of $Re_D = 50 \times 10^5$ and freestream turbulence of about 0.2%. This corresponds to prescribing the inlet boundary with uniform velocity of 18.6 m/s. In addition, turbulence intensity at the inlet was defined as 0.002 with a length scale of 0.04 m (corresponding to approximately $0.1D$) following previous computations in Dassanayake et al. [8]. Similarly, the ground was specified as a no-slip wall boundary condition with a moving velocity equal to 18.6 m/s. As the wheels are rotating, a no-slip condition with angular velocity of 89.44 rad/s were prescribed (corresponding to moving ground velocity of 18.6 m/s) for the wheel boundaries. The top boundary was defined as a

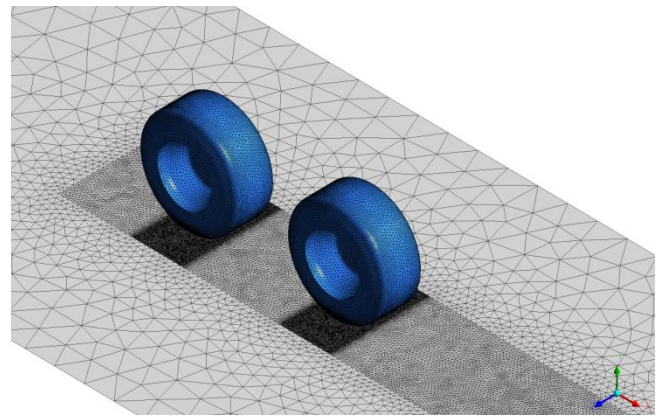
free-slip wall, while both side walls were set with symmetry boundary conditions. A zero (atmospheric) pressure was prescribed at the outlet.



(a)



(b)



(c)

Fig. 2: Computational grid used in the present study: (a) overall grid showing finer grids within inner block enclosing wheels (b) close-up of boundary layer mesh around wheels and moving ground (c) grids on wheels and moving ground.

2.4 Turbulence Modelling

Previous computational studies using URANS had employed one-equation Spallart-Almaras and two-equations Realizable $k-\epsilon$ (RKE) models (for instance, in McManus and Zhang [5] and Axerio et al. [9]), and also the two-equation $k-\omega$ Shear Stress Transport (SST) model (for example, in Leśniewicz et al. [7] and Dassanayake et al. [8]), which has shown better prediction in near-wall flow separations. Although URANS models were able to predict aerodynamics forces and mean flow structures in previous wheel studies, they are limited in accurately resolving the wide range of length and time scales in turbulence structures, leading to excessively large scale predictions [13,14]. In the present study, we employed a scale resolving (SRS) or scale adaptive (SAS) SST model to simulate the turbulence for flow around rotating wheels. SRS or SAS models includes the von Kármán length-scale, allowing the model to adjust to turbulence structures that could be resolved, resulting in LES-like simulation [12].

2.5 Computational Procedure

Unsteady simulation for both single and tandem wheel cases were initiated from a prior steady-state solution. A time-step of 0.00001s was used, resulting in a Courant number of the order $O(0)$ and a non-dimensionalized time-step ($\Delta t U/D$) of approximately 0.00045. The time-step is smaller than in previous URANS studies and is selected as more stable unsteady solutions were sought. All

unsteady simulations were allowed to run for at least 1200 non-dimensional time units and results were time-averaged from the final few periods. In all simulations, a second-order backward Euler scheme is employed for the temporal discretization and a high resolution method is used for the advection scheme.

3. Results and Discussion

In this section, results for a rotating single wheel in contact with the ground is presented, followed by results for the rotating tandem wheel case.

3.1. Single Wheel

We begin by presenting the results for the benchmark isolated or single wheel case. Figure 3 compares the surface pressure coefficient at centerline of the single wheel with experimental data of Fackrell [10] (in [5,8]). Surface pressure coefficient is defined as $C_p = (p - p_\infty)/(0.5\rho U_\infty^2)$ where p is local pressure at location of interest, p_∞ is a far-field reference pressure, ρ is fluid density and U_∞ is free stream velocity. Both SST and SAS-SST turbulence model were run in the present study for comparison purposes.

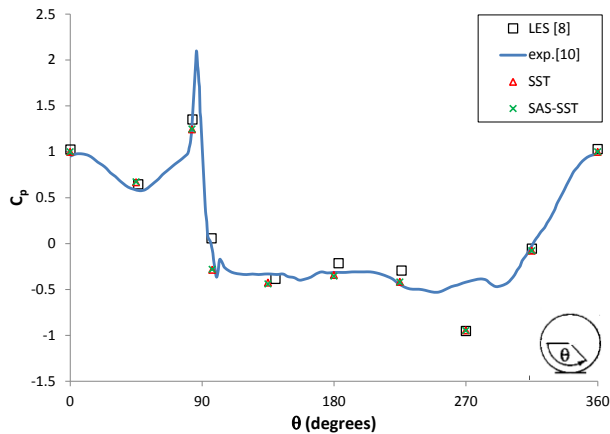
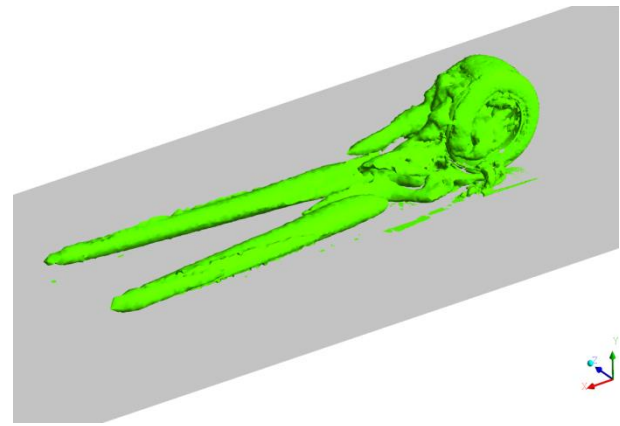


Fig. 3: Distribution of surface pressure coefficient at centerline of single wheel in comparison to experimental results [10] and LES results [8]. Position angle around wheel is defined per inset legend courtesy of McManus & Zhang [5].

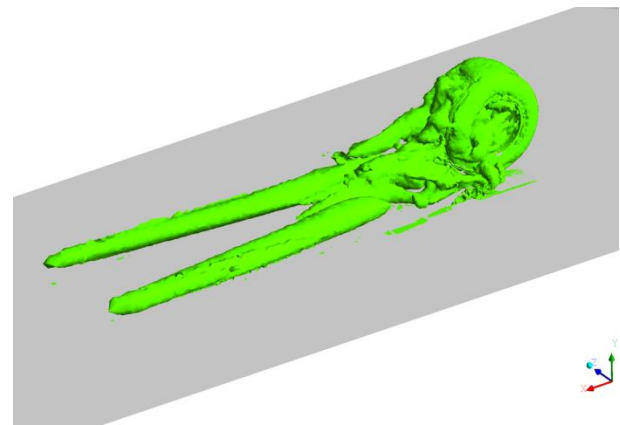
Figure 3 shows reasonable agreement of present model with previous experimental data, including at region close to wheel-ground contact patch, except at the upper region of the single wheel (i.e $\theta = 270^\circ$). However, this lower surface pressure predicted at $\theta = 270^\circ$ position, using both SST and SAS-SST model, is in good agreement with LES results obtained in Dassanayake et al. [8]. Integrating surface pressure, the total pressure lift and drag forces on a single wheel are presented in Table 1. Drag coefficients (C_D) predicted in the present model correspond well with experimental results. However, lift coefficients (C_L) are overpredicted by the present model, which is likely influenced by the lower pressure magnitude predicted in the upper region of the wheel. Both drag and lift coefficient are defined respectively as $C_D = F_x/(0.5\rho U_\infty^2 A)$ and $C_L = F_y/(0.5\rho U_\infty^2 A)$, where F_x is the streamwise force computed by integrating the fluid stresses acting in the x-direction on the tyre surface, F_y is the vertical force computed by integrating the fluid stresses acting in the y-direction on the tyre surface and A is the frontal area of the tyre. For consistent comparison with previous works, it is remarked that for Table 1, only the pressure component is considered for fluid stresses.

Table 1: Total pressure lift and drag coefficients for rotating single wheel

Case	C_L	C_D
Present model (SST)	0.37	0.53
Present model (SAS-SST)	0.38	0.54
S-A [5]	0.15	0.47
RKE [5]	0.16	0.43
Experiment [10]	0.28	0.51



(a)



(b)

Fig. 4: Vortical structures around a single wheel based on a constant λ_2 -criterion: (a) SST model (b) SAS-SST model.

Figure 4 presents the vortical structures predicted in the present model using the λ_2 -criterion technique [15]. Both SST and SAS-SST models show large pair of counter-rotating vortices dominating the downstream wake region of a single wheel and flow 'jetting' to lower sides of the wheel as flow is forced out from the wheel-ground contact region. This corresponds well with typical flow structures expected around a rotating wheel. Although little separate the surface pressure results between the present SST and SAS-SST models, Figure-4 shows some slight difference in predicted vortical structures, especially in the lower wake region of a single wheel. At similar constant λ_2 -levels, SAS-SST model predicts slightly larger vortical structures and more detailed flow structures at the lower sides of the single wheel, compared to SST model. For the tandem wheel, we proceed with SAS-SST computations to model the turbulent flow.

3.2. Tandem wheels

Total lift and drag forces on both rotating front and rear wheel is summarized in Table 2. Here, both pressure and shear stress contribution are considered in computing the streamwise and vertical forces acting on the tyre. In comparison to the front wheel (and also single isolated wheel case), drag coefficient on the rear wheel is lowered, and a negative lift (downforce) is experienced by the rear wheel. In addition, under a tandem wheel configuration, the front wheel exhibits reduced lift compared to the isolated single wheel case.

Table 2: Total lift and drag coefficients for rotating tandem wheels

Case	C_L	C_D
Front wheel	0.19	0.55
Rear wheel	-0.14	0.37

Figure 5 shows the vortical structures present in a tandem wheel case, as flow around the rotating front wheel interacts with the rotating rear wheel. In the gap between the wheels, much complex vortical structures are present and the pair of counter-rotating vortical structure from the lower wake region of the front wheel is reduced in length while flowing besides the lower rear wheel sides. Vortical structures between the wheels are low pressure regions, which are likely to induce lower drag on the rear wheel.

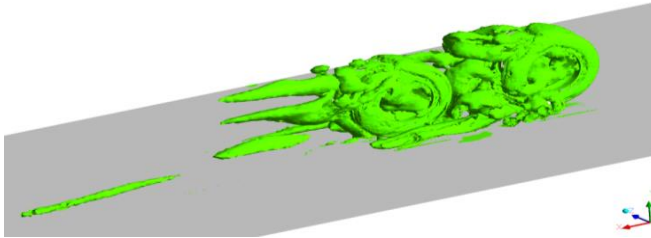
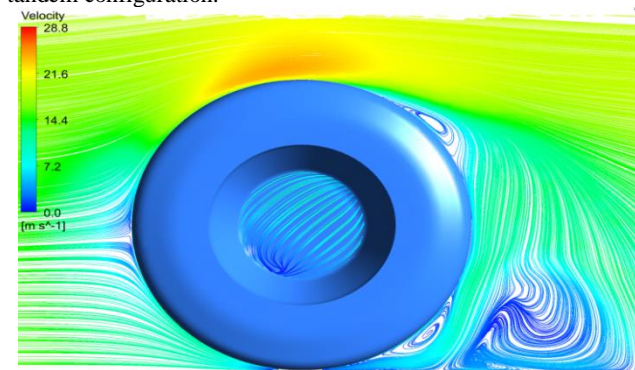
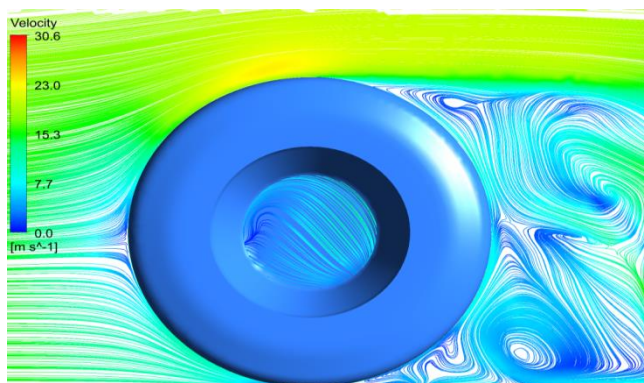


Fig. 5: Vortical structures in a rotating tandem wheel case based on a constant λ_2 -criterion.

Figure 6 shows that larger rear vortices are attached to the lower front wheel in the tandem wheel case compared to the single wheel case. Streamlines in Figure 6 also indicate earlier separation location in the upper wheel region for the tandem configuration in contrast to the single wheel case. It is hypothesised that this is influenced by the interaction of flow from the rotating rear wheel, hence, likely contributing to the lower lift of the front wheel in a tandem configuration.



(a)



(b)

Fig. 6: Streamlines around rotating front wheel for: (a) isolated single wheel (b) tandem wheels.

4. Conclusion

Flow around rotating single and tandem wheels in contact with the ground was computationally investigated using unsteady scale-adaptive shear stress transport (SAS-SST) simulation. Wheel geometry used was based on an actual slick tyre used in the bench-

mark experiments of Fackrell and Harvey [6,10] and the gap between tandem wheels was fixed at 0.5D. Good agreement between the present model and experimental data for the single wheel were obtained except at the upper region of the wheel, which on the other hand corresponded well with a previous LES study. The tandem wheel results indicated that the rear wheel experiences lower drag and negative lift compared to the front wheel. Lift coefficients on the front wheel was also reduced compared to the single wheel case, highlighting likely influence of having a rotating rear wheel in proximity of the front wheel. Future investigation to examine influence of varying gap between front and rear wheels on the flow and aerodynamic forces on tandem wheels is recommended for further study.

Acknowledgement

The authors would like to gratefully acknowledge financial support provided by Universiti Kebangsaan Malaysia (under project grant ID: GGPM 2013-092) and Ministry of Higher Education (under project grant FRGS/2/2013/TK01/UKM/02/2).

References

- [1] Agathangelou B & Gascoyne M (1998), Aerodynamic Design Considerations of a Formula 1 Racing Car. *SAE International Congress and Exposition* (Detroit, Michigan, U.S.A), pp. 23–26, SAE Paper No. 980399.
- [2] Wickern G, Zwicker K & Pfadenhauer M (1997), Rotating wheels - their impact on wind tunnel test techniques and on vehicle drag results. *SAE Int.* 970133.
- [3] Mlinaric P (2007), Investigation of the Influence of Tyre Deformation and Tyre Contact Patch on CFD Predictions of Aerodynamic Forces on a Passenger Car (Gothenburg: Chalmers University of Technology).
- [4] Nelson PM & Phillips SM (1997), Quieter Road Surfaces. Transport Research Laboratory Annual Review 1997, Transport Research Laboratory, Crowthorne, U.K.
- [5] McManus J & Zhang X (2006), A computational study of the flow around an isolated wheel in contact with the ground. *J. of Fluids Eng.* 128, pp. 520-530.
- [6] Fackrell JE & Harvey JK (1975), The Aerodynamics of an Isolated Road Wheel in Pershing, B., editor, *Proceedings of the Second AIAA Symposium of Aerodynamics of Sports and Competition Automobiles* (Los Angeles, California, U.S.A., 11 May), pp. 119–125.
- [7] Leńiewicz P, Kulak M & Karczewski M (2014), Aerodynamic analysis of an isolated vehicle wheel. *Journal of Physics: Conference Series* 530, 012064.
- [8] Dassanayake PRK, Ramachandran D, Salati L, Barber TJ & Doig GC (2012), Unsteady computational simulation of the flow structure of an isolated wheel in contact with the ground. *Proceedings of the 18th Australasian Fluid Mechanics Conference* (Launceston, Australia), pp. 3-7.
- [9] Axerio J, Iaccarino G, Issakhanian E, Lo K, Elkins C & Eaton J (2009), Computational and Experimental Investigation of the Flow Structure and Vortex Dynamics in the Wake of a Formula 1 Tire. SAE Technical Paper 2009-01-0775.
- [10] Fackrell JE (1974), The Aerodynamics of an Isolated Wheel Rotating in Contact With the Ground. Ph.D. thesis, University of London, U.K.
- [11] Spagnolo S, Zhang X, Hu Z, Stalnov O & Angland D (2017), Unsteady aerodynamics of single and tandem wheels. *Journal of Fluids and Structures* 69, pp. 121-136.
- [12] Menter FR & Egorov Y (2005), A Scale-Adaptive Simulation Model using Two-Equation Models. AIAA paper 2005-1095.
- [13] Shim YM, Sharma RN & Richards PJ (2009), Numerical study of the flow over a circular cylinder in the near wake at Reynolds number 3900. AIAA paper 2009-4160.
- [14] Derakhshandeh JF, Arjomandi M, Dally B & Cazzolato B (2014), The effect of arrangement of two circular cylinders on the maximum efficiency of Vortex-Induced Vibration power using a Scale-Adaptive Simulation model. *Journal of Fluids and Structures* 49, pp. 654–666.
- [15] Barbone L, Gattei L & Rossi R (2005), Identification and analysis of turbulent structures around a simplified car body. *Proceedings of the 2nd European Automotive CFD Conference* (Frankfurt, Germany).